Dynamic chest radiography: clinical validation of ventilation and perfusion metrics derived from changes in radiographic lung density compared to nuclear medicine imaging

Rie Tanaka[1]^, Isao Matsumoto[2], Masaya Tamura[2], Munehisa Takata[2], Shuhei Yoshida[2], Daisuke Saito[2], Yusuke Tanaka[2], Dai Inoue[3], Noriyuki Ohkura[4], Kazuo Kasahara[4]

[1]College of Medical, Pharmaceutical & Health Sciences, Kanazawa University, Kanazawa, Ishikawa, Japan; [2]Department of Thoracic Surgery, Kanazawa University, Kanazawa, Ishikawa, Japan; [3]Department of Radiology, Kanazawa University Hospital, Kanazawa, Ishikawa, Japan; [4]Department of Respiratory Medicine, Kanazawa University Hospital, Kanazawa, Ishikawa, Japan

Contributions: (I) Conception and design: R Tanaka; (II) Administrative support: I Matsumoto, K Kasahara; (III) Provision of study materials or patients: M Tamura, M Takata, S Yoshida, D Saito, Y Tanaka, N Ohkura; (IV) Collection and assembly of data: M Tamura, M Takata, S Yoshida, D Saito, Y Tanaka, N Ohkura; (V) Data analysis and interpretation: R Tanaka, D Inoue; (VI) Manuscript writing: All authors; (VII) Final approval of manuscript: All authors.

Correspondence to: Rie Tanaka, PhD. College of Medical, Pharmaceutical & Health Sciences, Kanazawa University. 5-11-80 Kodatsuno, Kanazawa, Ishikawa, 920-0942 Japan. Email: rie44@mhs.mp.kanazawa-u.ac.jp.

Background: Dynamic chest radiography (DCR) is a type of non-contrast-enhanced functional lung imaging with a dynamic flat-panel detector (FPD). This study aimed to assess the clinical significance of ventilation and perfusion metrics derived from changes in radiographic lung density on DCR in comparison to nuclear medicine imaging-derived metrics.

Methods: DCR images of 42 lung cancer patients were sequentially obtained during respiration using a dynamic FPD imaging system. For each subdivided lung region, the maximum change in the averaged pixel value (Δ_{max}), i.e., lung density, due to respiration and cardiac function was calculated, and the percentage of Δ_{max} relative to the total of all lung regions ($\Delta_{max}\%$) was computed for ventilation and perfusion, respectively. The $\Delta_{max}\%$ was compared to the accumulation of radioactive agents such as Tc-99m gas and Tc-99m macro-aggregated albumin (radioactive agents%) on ventilation and perfusion scans in the subdivided lung regions, by Spearman's correlation coefficient (r) and the Dice similarity coefficients (DSC). To facilitate visual evaluation, $\Delta_{max}\%$ was visualized as a color scaling, where larger Δ_{max} values were indicated by higher color intensities.

Results: We found a moderate correlation between $\Delta_{max}\%$ and radioactive agents% on ventilation and perfusion scans, with perfusion metrics (r=0.57, P<0.001) showing a higher correlation than ventilation metrics (r=0.53, P<0.001). We also found a good or strong correlation (r≥0.5) in 80.9% (34/42) of patients for perfusion metrics (r=0.60±0.16) and in 52.4% (22/42) of patients for ventilation metrics (r=0.53±0.16). DSC indicated a moderate correlation for both metrics. Decreased pulmonary function was observed in the form of reduced color intensities on color-mapping images.

Conclusions: DCR-derived ventilation and perfusion metrics correlated reasonably well with nuclear medicine imaging findings in lung subdivisions, suggesting that DCR could provide useful information on pulmonary function without the use of radioactive contrast agents.

Keywords: Diagnostic imaging; perfusion; radiography; thorax; ventilation

---

^ ORCID: 0000-0002-9476-5287.

Introduction

In the last two decades, there have been significant advances in functional and molecular imaging for the evaluation of pulmonary ventilation and perfusion. These techniques provide a wealth of information regarding pulmonary physiology, not for the entire lung as a unit [as does pulmonary function testing (PFT)], but on a regional level. Currently, nuclear medicine techniques, such as single-photon emission computed tomography (SPECT), are the clinical standard for pulmonary function imaging (1,2). However, nuclear medicine imaging techniques are expensive, have limited availability, and require radiopharmaceutical management. Conversely, four-dimensional CT (4DCT) (3-9) and cine magnetic resonance imaging (MRI) (10-12) have demonstrated promising results in the field of thoracic diagnosis and radiation therapy. While, there have been also much needs for promptly available functional lung imaging that are amenable to daily clinical and bedside use. There are many reports on the development of lung densitometry and digital fluoroscopic approaches (13-18), and these approaches have been shown to be useful for the evaluation of pulmonary ventilation and perfusion. However, these techniques have not expanded beyond their experimental phase because of technical limitations, including small field-of-view (FOV), poor image quality, and the necessity for special equipment.

Recently, advances in digital radiography technology have led to the development of dynamic chest radiography (DCR), which involves sequential imaging based on a dynamic flat-panel detector (FPD) in combination of low-dose pulsed X-ray (19). The main features of DCR are that it can be conducted with a total radiation dose less than that of conventional chest radiography, and that sequential chest radiographs can be obtained during respiration and cardiac beating at 15–30 frames per second (fps). A commercial DCR system was cleared by the US Food and Drug Administration in 2019 and is now available for clinical use in Japan and the USA (20). DCR will therefore be used in the clinical setting, as part of routine chest radiography. DCR provides a large amount of functional information on rib and diaphragm motion, cardiac motion, pulmonary ventilation, and perfusion. Several studies have reported potential clinical use for DCR (21-28), focusing on motion analysis of lung structures. Notably, pulmonary ventilation and perfusion are reflected as time changes in radiographic lung density on DCR images. These changes are induced by relative changes in the blood volume, and/or in the volume of lung vessels and bronchi per unit lung volume (29,30). Therefore, pulmonary function could be assessed based on a dynamic analysis of radiographic lung density at successive times.

In 2006, lung density-based ventilation DCR was first reported (21). Thenceforth, image-processing techniques for DCR have improved, and several animal and clinical researches have reported the feasibility of using DCR for evaluating pulmonary ventilation and perfusion. For example, recent animal studies have indicated that changes in radiographic lung density correlated strongly with both blood and inspired air volume, and that functional abnormalities such as limited air flow, trapped air, and pulmonary embolism, could be detected as decreased changes in radiographic lung density, even with no use of radiopharmaceutical and contrast agents (30,31). Moreover, a preliminary clinical study found a high correlation between changes in radiographic lung density and the total accumulation of radioactive agents at the lobar/whole-lung level, and demonstrated the feasibility of DCR-derived ventilation-perfusion studies (32). These findings highlight the ability of DCR to provide ventilation and perfusion metrics on the basis of changes in radiographic lung density. However, the diagnostic performance of DCR in lung subdivisions remains unknown. To allow further clinical implementation, it needs to be determined whether DCR could quantitatively evaluate pulmonary function in each lung subdivision.

Thus, this study aimed to assess the clinical significance of ventilation and perfusion metrics derived from changes in radiographic lung density in lung subdivision, during respiration and cardiac function on DCR compared to nuclear medicine imaging-derived metrics.

Methods

Subjects

This single-site clinical study involved 42 consecutive

4018

Tanaka et al. DCR- versus unclear medicine imaging-derived metrics

inpatient and out-patients in thoracic surgery at our institution. Patients were retrospectively recruited if they had conducted DCR, nuclear medicine imaging, i.e., ventilation and perfusion scans, and PFT within 3 months of each other (age 51–88 years, mean age 73 years, male-to-female ratio 31:11). No patient underwent thoracic surgery or treatments between sessions. The averaged interval between DCR and nuclear medicine imaging was 17.9 days (range, 0–65 days, median: 16 days).

The study was conducted in accordance with the Declaration of Helsinki (as revised in 2013). This study was approved by our institutional review board (registration number 1729), and all patients provided informed consent for study participation.

DCR

Sequential chest radiographs of 42 lung cancer patients were acquired by a dynamic digital radiography system (prototype model), consisting of a dynamic FPD (PaxScan 4343CB; Varex Imaging Corporation, Salt Lake City, UT, USA), and an X-ray generator/tube (DHF-155H II/UH-6QC-07E, Hitachi, Ltd., Chiyoda, Japan). Imaging was performed during forced breathing of about 14 s (5-s expiration, 2-s breath-holding, 5-s inspiration, and 2-s breath-holding). Except for the breathing, the setting was the same as for conventional chest radiography; the imaging was performed in a posteroanterior (PA) direction with the patient in a standing position. Details of DCR have been described previously (19,32). The patients were instructed to take a forced breathing under automated voice guidance. The imaging conditions were as follows: 100 kV, 0.2 mAs/pulse, 15 fps, source-to-image distance =200 cm, FOV =43 cm × 43 cm, resulting in approximately 210 frames of DCR images. The total surface entrance dose was less than the guidance level for two projections (PA + lateral) (1.9 mGy) (33,34). The matrix size was 1,024×1,024 pixels, the pixel size was 417×417 μm^2, and the gray-scale image range was 16 bits. In our preliminary experiment, we confirmed high linearity between the X-ray dose (detector's input) and pixel values (detector's output) by plotting their relationship. The pixel values were inverted, so that high pixel values were related to bright (i.e., white) areas in the images, indicating high X-ray absorption.

Image analysis

Ventilation and perfusion metrics were generated by

measuring regional changes in radiographic lung density on DCR images, which are due to respiration and cardiac function. For all frames of DCR images, the lung fields were segmented by a semantic segmentation algorithm (35,36), and the regions outside of the lung regions were replaced with a pixel value of 0 to be excluded from image analysis. Thereafter, the lung area was measured to determine a representative image frame showing the average lung area in all image frames. On a representative image frame, each lung was divided into equal 5×12 grid-shaped regions, resulting in a total of 10×12 grid-shaped regions for both lungs. For other image frames, the divided lung regions were linearly transformed corresponding to the lung scaling area during respiration, in order to measure the average pixel values in each grid-shaped region throughout all frames. All procedures were conducted using home-built programs (C^{++}BuilderXE8; Embarcadero Technologies, Austin, TX, USA).

Figure 1 shows the changes in radiographic lung density observed on DCR images and its quantification approach for this study. As shown in *Figure 1A*, the changes due to respiration and cardiac function are reflected as two different types of periodic changes in pixel value on DCR images. To compute the changes in pixel value for each factor of ventilation and perfusion, respectively, the changes were separated based on differences in their spatial frequency (32,37). Subsequently, the maximum density changes in the averaged pixel value (Δ_{max}) was determined in each 10×12 grid-shaped region. The percentage of Δ_{max} of each lung region relative to that of the total lung ($\Delta_{max}\%$) was then calculated using the following equation:

$$\begin{aligned} &\Delta_{max} \text{ of each lung region (\%) } (\Delta_{max}\%)\\ &= \frac{\Delta_{max} \text{ in each lung region}}{\text{Total of } \Delta_{max} \text{ in all lung regions}} \times 100 \text{ (\%)} \end{aligned} \quad [1]$$

Thereafter, ventilation $\Delta_{max}\%$ (V) and perfusion $\Delta_{max}\%$ (Q) were provided in a range of 0–100 for comparison with nuclear medicine imaging-derived metrics at a subdivided lung level. To facilitate visual evaluation, $\Delta_{max}\%$ was visualized as a color scaling, where larger Δ_{max} values were indicated by higher color intensities (hereafter, color-mapping images). The degree of color transparency on color-mapping images was determined based on normalized $\Delta_{max}\%$, derived by dividing $\Delta_{max}\%$ in each subdivision by the maximum $\Delta_{max}\%$ of all subdivided lung regions. Normalized $\Delta_{max}\%$ ranged from 0.0 to 1.0, from transparent to solid color; on a region-by-region basis throughout the lung, this produces color-mapping images as shown in *Figure 1B* (*Video 1*).
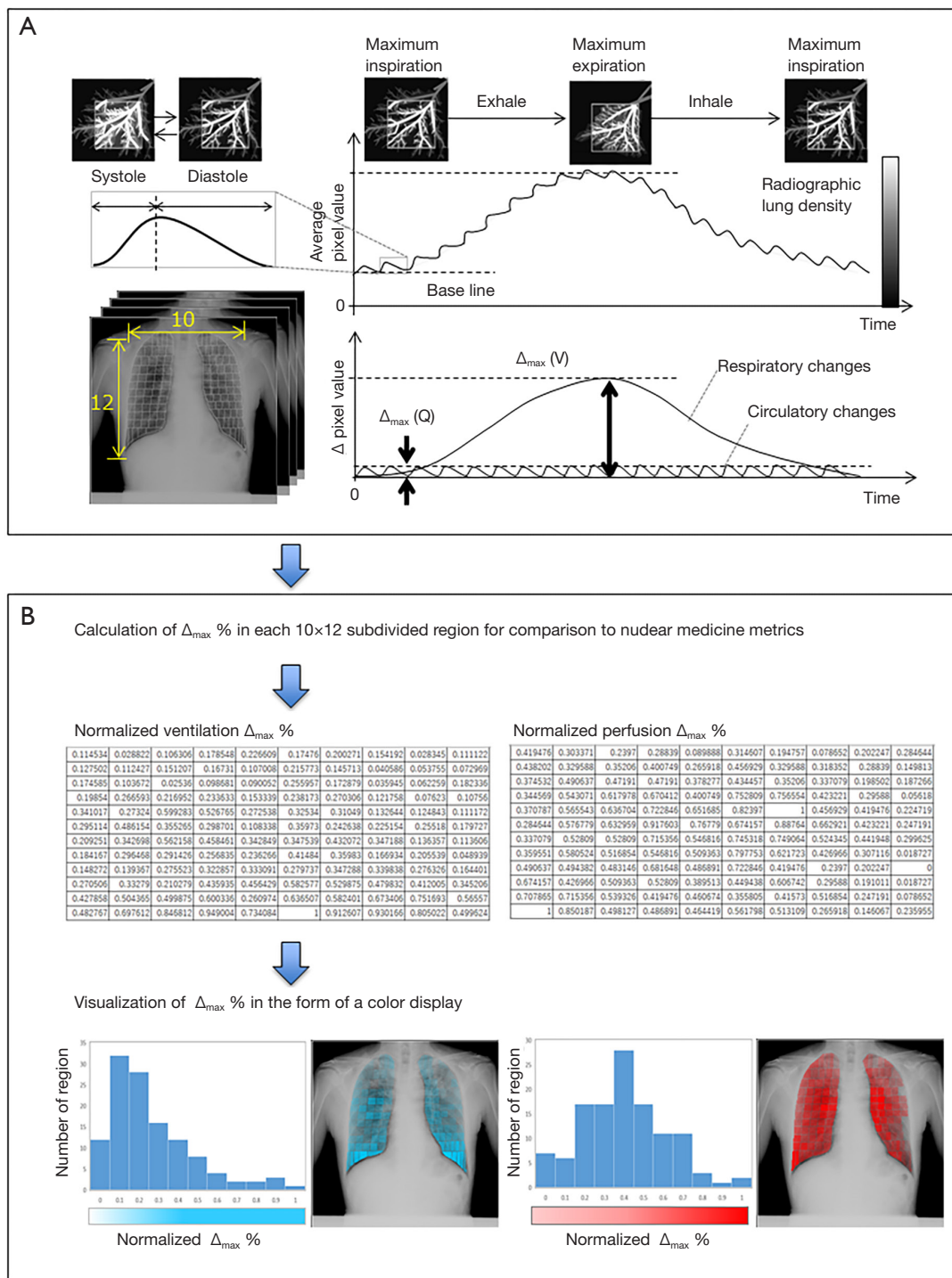
Figure 1 Overall algorithm for generating ventilation and perfusion metrics based on dynamic chest radiography (DCR). (A) Periodic changes in radiographic lung density due to respiration and cardiac function, measured in each grid-shaped region, schematically presented on DCR images (10×12 regions). (B) Procedures for creating color-mapping based on normalized Δ_{max} from 0–1 (from transparent to solid color); light blue indicates respiration and red indicates perfusion. Δ_{max}, maximum change in the averaged pixel value.

4020

Tanaka et al. DCR- versus unclear medicine imaging-derived metrics
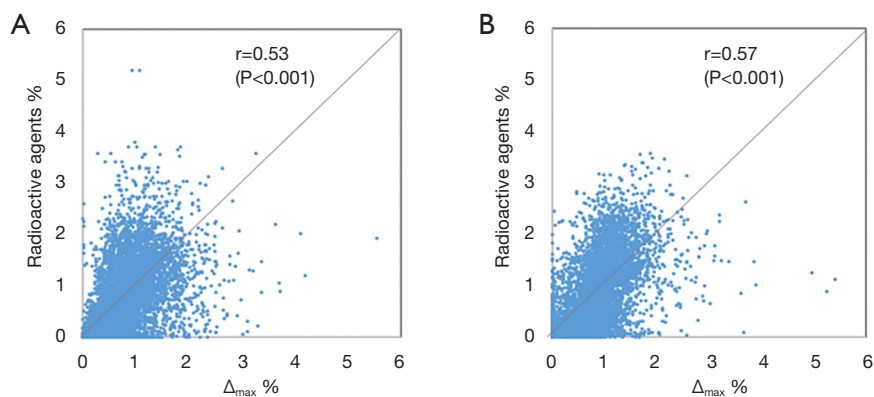
Figure 2 Scatter plots showing the comparison between (A) changes in radiographic lung density (Δ_{max}%) due to ventilation and rate of accumulation of radioactive agents (radioactive agents%) measured on ventilation scans, and (B) Δ_{max}% due to cardiac function and radioactive agents% measured on perfusion scans, with 5,040 plots across all 42 patients, respectively. Δ_{max}% and radioactive agents% were positively correlated. The line y = x (black) is a reference for perfect agreement on each plot. The overlaid white text indicates Spearman's correlation coefficient (r).

Lung scans

The nuclear medicine scans were acquired on SPECT/ CT scanners (Siemens Symbia T6, Siemens Healthcare, Erlangen, Germany), or SPECT cameras with cadmium-zinc-telluride (CZT) detectors (Discovery NM/CT 670 CZT, GE Healthcare, Chicago, IL, USA) using Tc-99m gas (370 MBq) and Tc-99m macro-aggregated albumin (200MBq) for ventilation and perfusion, respectively. For each patient, we conducted image registration between DCR and nuclear medicine images, using a landmark-based method. Nuclear medicine scan images were vertically and horizontally shifted and/or rotated in the vertical and horizontal directions using custom-written software, for matching to DCR images using the landmarks. Subsequently, the total accumulation of radioactive agents was calculated in each lung region on a frontal view for ventilation and perfusion scans. The rate of radioactivity accumulation in each lung region was determined relative to the total accumulated radioactive agents in both lungs (radioactive agents%) on ventilation and perfusion scans, respectively.

Statistical analysis

Spearman's correlation coefficient (r) between Δ_{max}% and radioactive agents% in each subdivided lung region was calculated using R software (version 4.0.2) (38). Similar to a previous study (39), the cutoff values proposed by Zou

et al. (40,41) were utilized to interpret Spearman's correlation coefficients: r=1.0 as perfect, 0.8≤r<1.0 as strong, 0.5≤r<0.8 as moderate, 0.2≤r<0.5 as weak, and 0≤r<0.2 as no correlation.

We also calculated the Dice similarity coefficient (DSC) for low-functional lungs (d_{30}), defined as the 0–30th percentile lung regions with the lowest ventilation or perfusion metrics (42), as well as healthy functional lungs (d_{31-100}), defined as the 31st–100th percentile lung regions, between Δ_{max}% and radioactive agents% for ventilation and perfusion, respectively, in each lung subdivision. For DSC, we used the following cutoff values: 0.8< DSC ≤1.0 as almost perfect, 0.6< DSC ≤0.8 as substantial, 0.4< DSC ≤0.6 as moderate, 0.2< DSC ≤0.4 as fair, 0≤ DSC ≤0.2 as slight, and DSC < 0 as poor overlap (40,43).

In addition, statistical analysis was performed to test whether there was a significant difference in correlations between males and females, using a two-sample two-tailed *t*-test (P<0.05).

Results

There was a moderate correlation between Δ_{max}% and radioactive agents% on both ventilation and perfusion scans, with perfusion metrics (r=0.57, P<0.001) showing a higher correlation than ventilation metrics (r=0.53, P<0.001), as shown in *Figure 2*. *Table 1* shows the mean and standard deviation (SD) of Spearman's r for each metric, for each sex. The mean ± SD (range) of r was 0.53±0.16

Table 1 Comparing average Spearman's correlation coefficients (r) values between $\Delta_{max}\%$ and the accumulated rate of radioactive agents (radioactive agents%) for ventilation and perfusion

Group	Ventilation	Perfusion
Male (n=31)	0.58±0.15, P<0.01	0.60±0.12 NS
Female (n=11)	0.40±0.16, P<0.01	0.51±0.21 NS
Total (n=42)	0.53±0.16	0.60±0.16

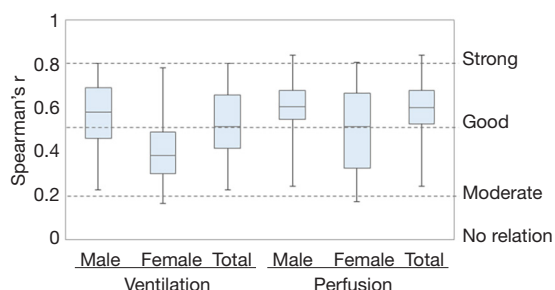Values are presented as the mean ± SD. NS, not significant.

Figure 3 Box plots of Spearman's correlation coefficients (r) between the percentage of maximum changes in pixel value ($\Delta_{max}\%$) and the accumulation rate of radioactive agents (radioactive agents%) for ventilation and perfusion (n=42; male-to-female ratio 31:11). The median, lower, and upper 25th percentile values for Spearman's r are shown for each box. The dotted horizontal lines show classification the Spearman's r values as r=1.0 indicates perfect, 0.8≤r<1.0 indicates strong, 0.5≤r<0.8 indicates moderate, 0.2≤r<0.5 indicates weak, and 0≤r<0.2 indicates no correlation.
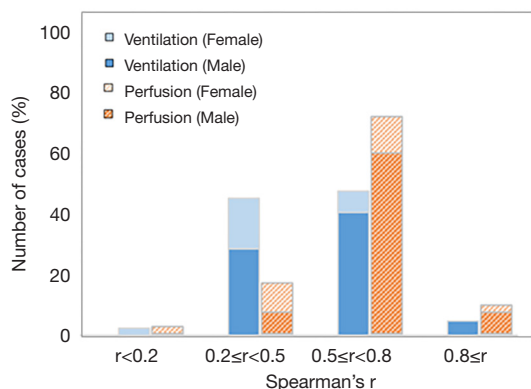

Figure 4 Bar graphs showing the number of cases of each sex for Spearman's correlation coefficient (r) (strong: 0.8≤r<1.0; good: 0.5≤r<0.8; moderate: 0.2≤r<0.5; no correlation: 0.0≤r<0.2) between $\Delta_{max}\%$ and the accumulation rate of radioactive agents (radioactive agents%) for ventilation and perfusion

(0.23–0.80) for ventilation and 0.60±0.16 (0.24–0.84) for perfusion. In terms of sex differences, males demonstrated higher correlations than females for both ventilation (male: r=0.58±0.15, female: r=0.40±0.16) and perfusion metrics (male: r=0.60±0.12, female: r=0.51±0.21), with a significant difference for ventilation metrics (P<0.01). *Figure 3* shows the box plots of Spearman's r between $\Delta_{max}\%$ and radioactive agents% for ventilation and perfusion for each sex. On the whole, there was a moderate or good correlation between $\Delta_{max}\%$ and radioactive agents% for both ventilation and perfusion, in every subgroup (male, female, and total). As shown in *Figure 4*, good or strong correlations were observed in 80.9% (34/42) of patients for perfusion metrics and in 52.4% (22/42) of patients for ventilation metrics.

Table 2 demonstrates a summary of the DSCs d_{30} for low-functional lungs and $d_{31\text{-}100}$ for healthy functional lungs in each subgroup (male, female, and total) for ventilation and perfusion metrics, respectively. In general, there was a moderate overlap between $\Delta_{max}\%$ and radioactive agents%. The d_{30} was 0.43±0.10 for ventilation and 0.52±0.10 for perfusion metrics, while the $d_{31\text{-}100}$ was 0.63±0.12 for ventilation and 0.65±0.12 for perfusion metrics. Although the difference was not statistically significant at the 0.05 level, males demonstrated higher DSCs than females for both ventilation and perfusion.

Figure 5 shows a representative example of a patient showing a good agreement between $\Delta_{max}\%$ and radioactive agents%, for both ventilation (r=0.73) and perfusion (r=0.84) (68-year-old man with postoperative right-lung cancer). Although right lobectomy led to a reduced percentage vital capacity, normal values for percentage forced expiratory volume in 1 second, ratio of forced expiratory volume in 1 second to forced vital capacity, and diffusing capacity of the lung for carbon monoxide implied normal function in the left lung (unaffected side). Both imaging modalities revealed a decreased ventilation and perfusion in the entire right lung. Qualitatively, DCR-derived color-mapping images indicated good visual concordance with nuclear medicine ventilation and perfusion scans.

Figure 6 shows representative images of a patient displaying poor agreement among the two metrics for ventilation (r=0.38) (69-year-old female with preoperative left-lung cancer). There was no ventilation and perfusion defect on nuclear medicine scans; however, color-mapping images revealed decreased $\Delta_{max}\%$ in the lower lung regions on and around the breast, resulting in lower color intensities on both ventilation and perfusion scans.

4022

Tanaka et al. DCR- versus unclear medicine imaging-derived metrics

Table 2 Comparison of average Dice similarity correlations (DSCs) d_{30} for low-functional lungs and d_{31-100} for healthy functional lungs between the maximum changes in pixel value (Δ_{max}%) and the accumulation rate of radioactive agents (radioactive agents%) for ventilation and perfusion

Group	d_{30} (low-functional lung)		d_{31-100} (healthy functional lung)	
	Ventilation	Perfusion	Ventilation	Perfusion
Male (n=31)	0.46±0.10 NS	0.54±0.12 NS	0.66±0.07 NS	0.66±0.06 NS
Female (n=11)	0.40±0.07 NS	0.42±0.10 NS	0.60±0.19 NS	0.61±0.20 NS
Total (n=42)	0.43±0.10 NS	0.52±0.11	0.63±0.12	0.65±0.12

NS, not significant. Values are given as the mean ± SD. In this study, DSCs were interpreted using the following criteria: 0.8< DSC ≤1.0 as almost perfect, 0.6< DSC ≤0.8 as substantial, 0.4< DSC ≤0.6 as moderate, 0.2< DSC ≤0.4 as fair, 0≤ DSC ≤0.2 as slight, and DSC <0 as poor overlap.
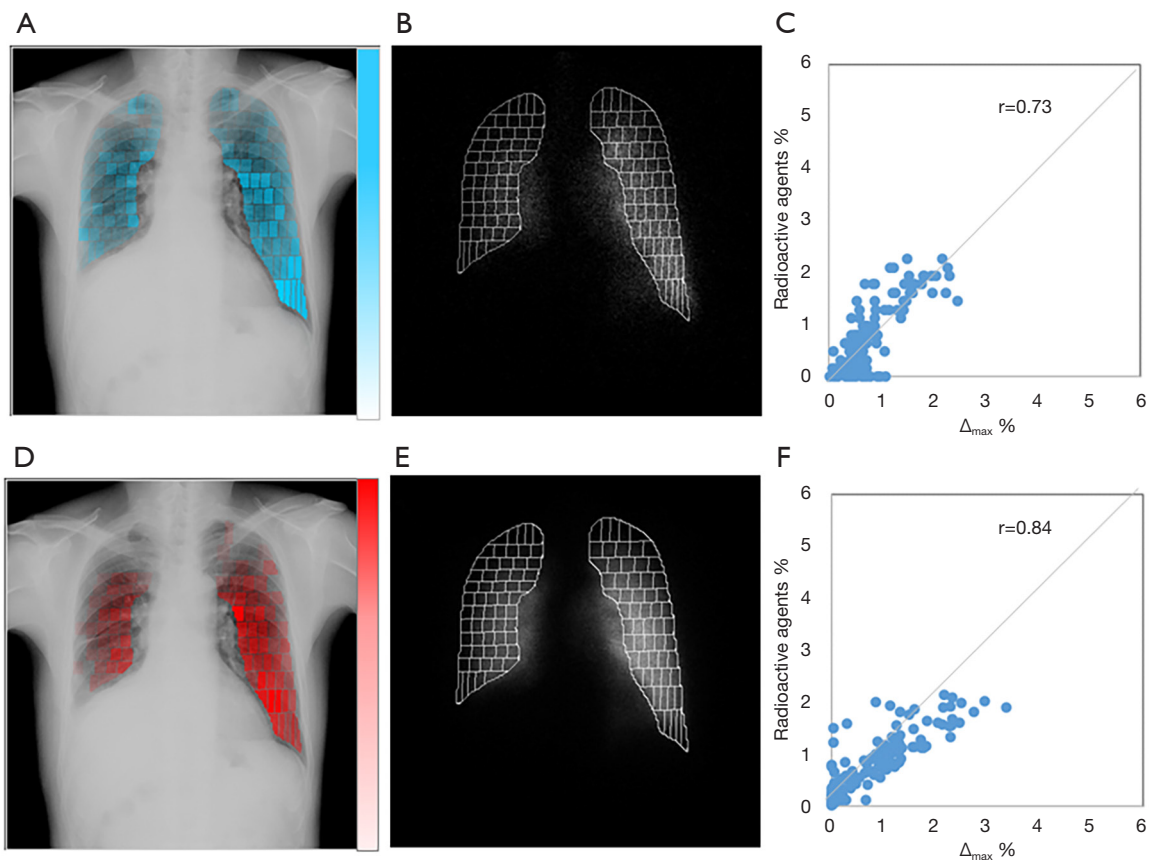

Figure 5 An example of a patient indicating good agreement between changes in radiographic lung density (Δ_{max}%) and the accumulation rate of radioactive agents (radioactive agents%) for both ventilation and perfusion. (A, D) The resulting color-mapping images; (B, E) the corresponding lung scans; and (C, F) a scatter plot for ventilation (upper row) and perfusion (lower row) of a 68-year-old man with postoperative right-lung cancer, VC (% predicted) 62.5, FEV1 (% predicted) 71.0, FEV1/FVC 93.3, and DLco (% predicted) 81.7 (*Video 1*). The color-mapping and nuclear medicine images demonstrate good agreement, with both images showing a decreased function in the right lung after lobectomy. DLco, diffusing capacity of the lung for carbon monoxide; FEV1, forced expiratory volume in 1 second; FEV1/FVC, ratio of forced expiratory volume in 1 second to forced vital capacity; VC, vital capacity.
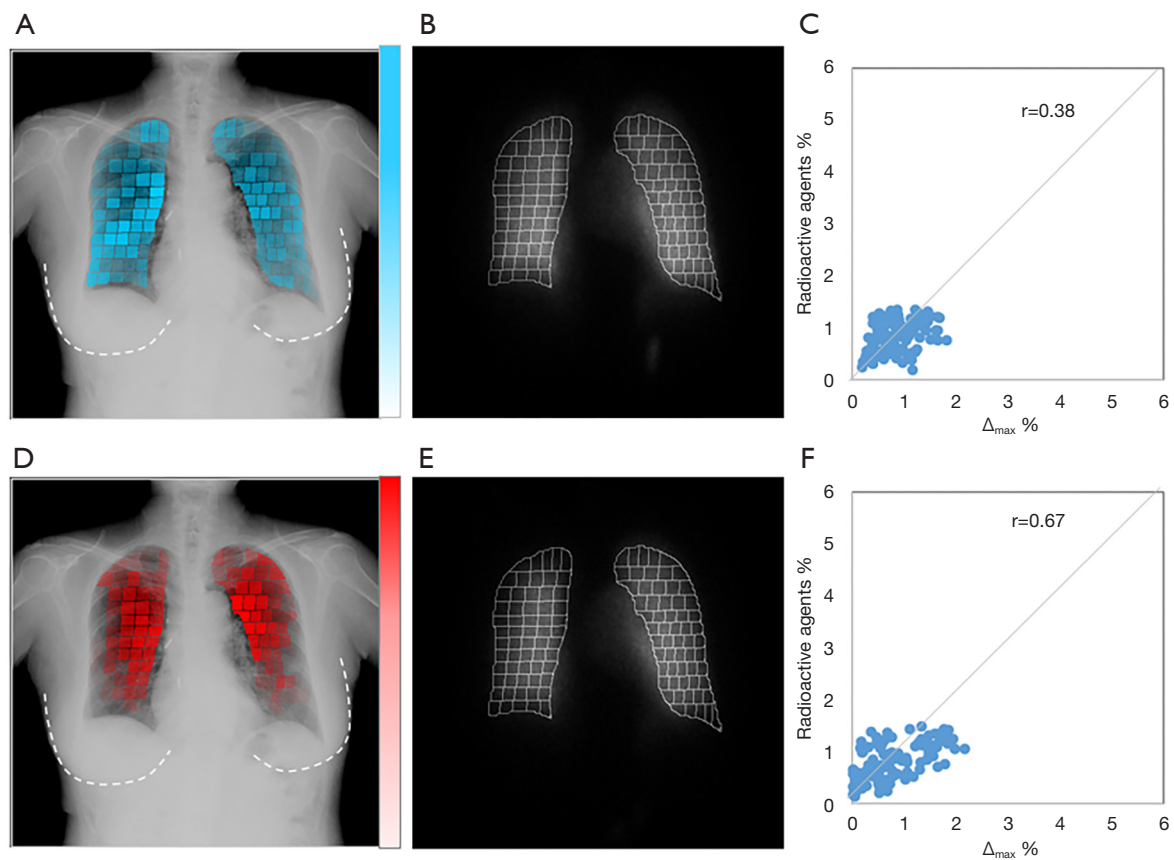
Figure 6 Examples of a patient displaying poor agreement between changes in radiographic lung density (Δ_{max}%) and the accumulation rate of radioactive agents (radioactive agents%) for both ventilation and perfusion. (A, D) The resulting color-mapping images; (B, E) the corresponding lung scans; and (C, F) a scatter plot for ventilation (upper row) and perfusion (lower row) of a 69-year-old female with preoperative left-lung cancer, showing specular lung nodule of 2 cm in diameter, in the left lower lobe (S8); VC (% predicted) is 136.8, FEV1 (% predicted) 120.6, FEV1/FVC 63.8, and DLco (% predicted) 81.7. The breast boundaries are traced by the dashed white lines. Color-mapping images demonstrate lower ventilation and perfusion in the lower lung, meanwhile the nuclear medicine scan images have no reduction in that area. DLco, diffusing capacity of the lung for carbon monoxide; FEV1, forced expiratory volume in 1 second; FEV1/FVC, ratio of forced expiratory volume in 1 second to forced vital capacity; VC, vital capacity.

Discussion

In this study, ventilation and perfusion metrics based on changes in radiographic lung density on DCR were validated in comparison to nuclear medicine imaging-derived metrics. No previous study has assessed the clinical significance of DCR-derived ventilation and perfusion metrics in lung subdivisions. We found that Spearman's r, DSCs, and color-mapping images indicated good or moderate overall agreement between Δ_{max}% and radioactive agents%, suggesting that changes in radiographic lung density correlated reasonably well with accumulated radioactive agents on lung scans. Additionally, decreased

pulmonary function was observed as reduced color intensities on color-mapping images, suggesting the ability of DCR to provide results that are clinically congruent with nuclear medicine imaging.

Our results provide additional evidence for those of previous researches reporting that radiographic lung density correlates strongly with both blood and inspired air volume in the lungs (29-32). A previous clinical study compared Δ_{max}% with radioactive agents% in each lung or in each lung third and found correlation coefficients in the order of 0.8 for each lung analysis and correlations in the range of 0.37–0.80 for each individual lung third. For the lower correlations in this study, averaging out pixel

values over large regions-of-interest could mitigate errors caused by mis-registration of images in comparisons at the lobar/whole-lung level. For a region-by-region evaluation of lung function with DCR, however, advanced non-rigid image registration (44,45) should be implemented, as was done in previous studies that compared 4DCT functional imaging with nuclear medicine imaging (3-13). For example, previous studies found correlations in the range of 0.22–0.76 between 4DCT-ventilation with positron-emission tomography-Galligas ventilation (5), and DSCs in the range of 0.1–0.60 between 4DCT-ventilation with SPECT perfusion defect (3). Although the current performance of DCR is less than that of 4DCT, DCR could be a comparable approach to 4DCT with further technical improvement in the future.

However, DCR have revealed several limitations in this study. The main limitation of DCR is the overlapped shadows on projection images due to a lack of 3D information. Overall, female patients demonstrated lower correlations between $\Delta_{max}\%$ and radioactive agents% than male patients. We confirmed that large mismatches were generally found in patients with large breasts; changes in radiographic lung density were likely to be reduced or eliminated in and around the breast on projection images, as shown in *Figure 6*. A second limitation of DCR is motion artifacts. On color-mapping images in some cases, we occasionally observed bright features in lung regions with pleural effusion and near the diaphragm edge, showing large respiratory displacement in the superior-inferior direction, resulting in false-negative results for ventilation impairments. With improved segmentation, and advanced image registration (44,45) and image processing techniques, such as the bone suppression technique (46-48), as well as a nonlinear image registration, the performance of DCR for the evaluation of pulmonary function could be further improved. A limitation in study design for this validation study was the difference in patient posture during DCR in standing and nuclear medicine lung scans in supine. The lungs have regional differences in the distribution of pulmonary blood and ventilation, due to gravity effects, which may be greater in the dependent part of the lungs (49). This might be a major factor for the decreased correlations in each lung subdivision between DCR-derived (standing) and nuclear medicine imaging-derived metrics (supine). Therefore, we plan to investigate DCR at the spine position in a future clinical study. In addition, there is a need to adapt diagnostic criteria based on the normal findings in radiographic lung density on DCR. To this end, further

clinical studies in a large number of patients are required to determine the physiological meaning of changes in radiographic lung density, and how these data can be applied in a clinical setting.

The main advantages of DCR are the lower imaging dose and greater accessibility, as compared to 4DCT, and that the total radiation dose is approximately as twice as that of conventional chest radiography. Although patients are still exposed to irradiation during the examination, this may be acceptable due to the greater information yield and given that DCR is a simple and rapid functional imaging procedure.

Conclusions

This study assessed the correlation between changes in radiographic lung density on DCR and accumulated radioactive agents on nuclear medicine images in subdivisions of the lung in lung cancer patients. We found that DCR-derived ventilation and perfusion metrics correlated reasonably well with findings on ventilation and perfusion scans in lung subdivisions. These results suggest that DCR could provide useful information related to pulmonary function, without the use of radioactive contrast agents.

Acknowledgments

Footnote

Conflicts of Interest: All authors have completed the ICMJE uniform disclosure form (available at http://dx.doi. org/10.21037/qims-20-1217). Dr. RT, Dr. IM, Dr. MT and Dr. KK report that this research was supported in part by a grant-in-aid for Scientific Research from the Ministry of Education, Culture, Sports, Science and Technology [#19K12841], and by Konica Minolta, Inc., Tokyo, Japan. Device used in our clinical study was also provided by

Ethical Statement: The authors are accountable for all aspects of the work in ensuring that questions related to the accuracy or integrity of any part of the work are appropriately investigated and resolved. The study was conducted in accordance with the Declaration of Helsinki (as revised in 2013). The study was approved by the Institutional Review Board of Kanazawa University (registration number 1729). Written informed consent was obtained from all individual participants.

References

1. Bajc M, Schümichen C, Grüning T, Lindqvist A, Roux RY, Alatri A, Bauer RW, Dilic M, Neilly B, Verberne HJ, Bolton RC, Jonson B. EANM guideline for ventilation/perfusion single-photon emission computed tomography (SPECT) for diagnosis of pulmonary embolism and beyond. Eur J Nucl Med Mol Imaging 2019;46:2429-51.

2. Hutton BF. The contribution of Medical Physics to Nuclear Medicine: looking back - a physicist's perspective. EJNMMI Physics 2014;1:2.

3. Castillo R, Castillo E, Martinez J, Guerrero T. Ventilation from four-dimensional computed tomography: density versus Jacobian methods. Phys Med Biol 2010;55:4661.

4. Yamamoto T, Kabus S, Klinder T, Lorenz C, Berg J, Blaffert T, Loo BW, Keall PJ. Investigation of four-dimensional computed tomography-based pulmonary ventilation imaging in patients with emphysematous lung regions. Phys Med Biol 2011;56:2279-98.

5. Kipritidis J, Siva S, Hofman MS, Callahan J, Hicks RJ, Keall PJ. Validating and improving CT ventilation imaging by correlating with ventilation 4D-PET/CT using 68Ga-labeled nanoparticles. Med Phys 2014;41:011910.

6. Yamamoto T, Kent MS, Wisner ER, Johnson LR, Stern JA, Qi L, Fujita Y, Boone JM. Single-energy computed tomography-based pulmonary perfusion imaging: Proof-of-principle in a canine model. Med Phys 2016;43:3998.

7. Vinogradskiy Y, Jackson M, Schubert L, Jones B, Castillo R, Castillo E, Guerrero T, Mitchell J, Rusthoven C, Miften M, Kavanagh B. Assessing the use of 4DCT-ventilation in pre-operative surgical lung cancer evaluation. Med Phys 2017;44:200-8.

8. Yamashiro T, Moriya H, Tsubakimoto M, Matsuoka S, Murayama S. Continuous quantitative measurement of the proximal airway dimensions and lung density on four-dimensional dynamic-ventilation CT in smokers. Int J Chron Obstruct Pulmon Dis 2016;11:755-64.

9. Ieko Y, Kadoya N, Kanai T, Nakajima Y, Arai K, Kato T, Ito K, Miyasaka Y, Takeda K, Iwai T, Nemoto K, Jingu K. The impact of 4DCT-ventilation imaging-guided proton therapy on stereotactic body radiotherapy for lung cancer. Radiol Phys Technol 2020;13:230-7.

10. Doganay O, Matin T, Chen M, Kim M, Mclntyre A, McGowan DR, Bradley KM, Povey T, Gleeson F. Time-series hyperpolarized xenon-129 MRI of lobar lung ventilation of COPD in comparison to V/Q-SPECT/CT and CT. Eur Radiol 2019;29:4058-67.

11. Doganay O, Chen M, Matin T, Rigolli M, Phillips JA, Mclntyre A, Gleeson F. Magnetic resonance imaging of the time course of hyperpolarized 129Xe gas exchange in the human lungs and heart. Eur Radiol 2019;29:2283-92.

12. O'Sullivan B, Couch M, Roche JP, Walvick R, Zheng S, Baker D, Johnson M, Botfield M, Albert MS. Assessment of repeatability of hyperpolarized gas MR ventilation functional imaging in cystic fibrosis. Acad Radiol 2014;21:1524-9.

13. Kourilsky R, Marchalm M, Marchal MT. A new method of functional x-ray exploration of the lungs: photoelectric stati-densigraphy. Dis Chest 1962;42:345-58.

14. George RB, Weill H, Tahir AH. Fluorodensimetric evaluation of regional ventilation in chronic obstructive pulmonary disease. South Med J 1971;64:1161-5.

15. Silverman NR. Clinical video-densitometry. Pulmonary ventilation analysis. Radiology 1972;103:263-5.

16. Lam KL, Chan HP, MacMahon H, Oravecz WT, Doi K. Dynamic digital subtraction evaluation of regional pulmonary ventilation with nonradioactive xenon. Invest

4026

Tanaka et al. DCR- versus unclear medicine imaging-derived metrics

Radiol 1990;25:728-35.

17. Bürsch JH. Densitometric studies in digital subtraction angiography: assessment of pulmonary and myocardial perfusion. Herz 1985;10:208-14

18. Kiuru A, Svedstrom E, Kuuluvainen I. Dynamic imaging of pulmonary ventilation. Description of a novel digital fluoroscopic system. Acta Radiol 1991;32:114-9.

19. Tanaka R. Dynamic chest radiography: flat-panel detector (FPD) based functional X-ray imaging. Radiol Phys Technol 2016;9:139-53.

20. Konica Minolta Healthcare Americas, Inc. Dynamic digital radiography. Accessed 31 Oct 2020. Available online: http://xraythatmoves.com/

21. Tanaka R, Sanada S, Okazaki N, Kobayashi T, Fujimura M, Yasui M, Matsui T, Nakayama K, Nanbu Y, Matsui O. Evaluation of pulmonary function using breathing chest radiography with a dynamic flat-panel detector (FPD): Primary results in pulmonary diseases. Invest Radiol 2006;41:735-45.

22. Yamada Y, Ueyama M, Abe T, Araki T, Abe T, Nishino M, Jinzaki M, Hatabu H, Kudoh S. Difference in diaphragmatic motion during tidal breathing in a standing position between COPD patients and normal subjects: Time-resolved quantitative evaluation using dynamic chest radiography with flat panel detector system ("dynamic X-ray phrenicography"). Eur J Radiol 2017;87:76-82.

23. Hida T, Yamada Y, Ueyama M, Araki T, Abe T, Nishino M, Jinzaki M, Hatabu H, Kudoh S. Time-Resolved quantitative evaluation of diaphragmatic motion during forced breathing in a health screening cohort in a standing position: dynamic chest phrenicography. Eur J Radiol 2019;113:59-65.

24. Ohkura N, Kasahara K, Watanabe S, Hara J, Abo M, Sone T, Kimura H, Takata M, Tamura M, Matsumoto I, Nakade Y, Sanada S, Tanaka R. Dynamic-Ventilatory Digital Radiography in Air Flow Limitation: A Change in Lung Area Reflects Air Trapping. Respiration 2020;99:382-8.

25. Tamura M, Matsumoto I, Saito D, Yoshida S, Takata M, Tanaka R, Takemura H. Dynamic chest radiography: Novel and less-invasive imaging approach for preoperative assessments of pleural invasion and adhesion. Radiology Case Reports 2020;15:702-4.

26. FitzMaurice TS, McNamara PS, Nazareth D, McCann C, Bedi R, Shaw M, Walshaw M. Utility and validity of dynamic chest radiography in cystic fibrosis (dynamic CF): an observational, non-controlled, non-randomised, single-centre, prospective study. BMJ Open Respir Res 2020;7:e000569.

27. Squire LF, Novelline RA. Overexpansion and collapse of the lung: causes of mediastinal shift. In: Mettler FA, ed. Fundamentals of Radiology. 4th ed. Cambridge, MA: Harvard University Press, 1988.

28. Fraser RS, Muller NL, Colman NC. Part III: Radiologic signs of chest disease. In: Fraser RS, Muller NL, Colman NC, Pare PD, eds. Fraser and Pare's Diagnosis of Diseases of the Chest. 4th ed. Philadelphia: W.B. Saunders, 1999.

29. Tanaka R, Tani T, Nitta N, Tabata T, Matsutani N, Muraoka S, Yoneyama T, Sanada S. Detection of pulmonary embolism based on reduced changes in radiographic lung density during cardiac beating using dynamic flat-panel detector: an animal-based study. Acad Radiol 2019;26:1301-8.

30. Tanaka R, Tani T, Nitta N, Matsutani N, Muraoka S, Yoneyama T, Sanada S. Pulmonary function diagnosis based on respiratory changes in lung density with dynamic flat-panel detector imaging: An animal-based study. Invest Radiol 2018;53:417-23.

31. Yamasaki Y, Abe K, Hosokawa K, Kamitani T. A novel pulmonary circulation imaging using dynamic digital radiography for chronic thromboembolic pulmonary hypertension. Eur Heart J 2020;41:2506.

32. Tanaka R, Matsumoto I, Tamura M, Takata M, Kasahara K, Ohkura N, Inoue D, Matsuura Y. Comparison of dynamic flat-panel detector-based chest radiography with nuclear medicine ventilation-perfusion imaging for the evaluation of pulmonary function: a clinical validation study. Med Phys 2020;47:4800-9.

33. International basic safety standards for protection against ionizing radiation and for the safety of radiation sources. In: IAEA Safety Series No. 115. Vienna: International Atomic Energy Agency (IAEA), 1996.

34. Annex IV. Schedule III. Guidance levels of dose, dose rate and activity for medical exposure. In: Radiological protection for medical exposure to ionizing radiation. Safety Guide. IAEA Safety Standards Series No. RS-G-1.5. p65. Vienna: International atomic energy agency (IAEA), 2002.

35. Kovacs W, Hsieh N, Roth H, Nnamdi-Emeratom C, Bandettini WP, Arai A, Mankodi A, Summers RM, Yao J. Holistic segmentation of the lung in cine MRI. J Med Imaging (Bellingham) 2017;4:041310.

36. Kitahara Y, Tanaka R, Roth H, Oda H, Mori K, Kasahara K, Matsumoto I. Lung segmentation based on a deep learning approach for dynamic chest radiography. Proc. of SPIE 10950. 109503M-1-7 2019. DOI: 10.1117/12.2512711.

37. Tanaka R, Matsuda H, Sanada S. Time-series analysis of lung texture on bone-suppressed dynamic chest radiograph for the evaluation of pulmonary function: a preliminary study. Proc. of SPIE 10137. 101371R 2017. DOI:10.1117/12.2254377.

38. R Development Core Team. R: A language and environment for statistical computing. Vienna, Austria. Accessed 31 Oct 2020. Available online: https://www.r-project.org

39. Yamamoto T, Kabus S, Berg JV, Lorenz C, Chung MP, Hong JC, Loo BW, Keall PJ. Reproducibility of four-dimensional computed tomography-based lung ventilation imaging. Acad radiol 2012;19:1554-65.

40. Zou KH, Tuncali K, Silverman SG. Correlation and simple linear regression. Radiology 2003;227:617-22.

41. Zou KH, Warfield SK, Bharatha A, Tempany CM, Kaus MR, Haker SJ, Wells WM, Jolesz FA, Kikinis R. Statistical validation of image segmentation quality based on a spatial overlap index. Acad Radiol 2004;11:178-89.

42. Yamamoto T, Kabus S, Lorenz C, Jhonston E, Maxim PG, Diehn M, Eclov N, Barquero C, Loo BW, Keall PJ. 4D CT lung ventilation images are affected by the 4D CT sorting method. Med Phys 2013;40:101907.

43. Landis JR, Koch GG. The measurement of observer agreement for categorical data. Biometrics 1977;33:159-74.

44. Klein S, Staring M, Murphy K, Viergever MA, Pluim JP. Elastix: a toolbox for intensity-based medical image registration. IEEE Trans Med Imaging 2010;29:196-205.

45. Metz CT, Klein S, Schaap M, Walsum T, Niessen WJ. Nonrigid registration of dynamic medical imaging data using nD + t B-splines and a groupwise optimization approach. Med Image Anal 2011;15:238-49.

46. Suzuki K, Abe H, MacMahon H, Doi K. Image-processing technique for suppressing ribs in chest radiographs by means of massive training artificial neural network (MTANN). IEEE Trans Med Imaging 2006;25:406-16.

47. Knapp J, Worrell S. Feature Based Neural Network Regression for Feature Suppression. U.S. Patent Number 204,292 B2, June 12 2012.

48. Kaji S, Kida S. Overview of image-to-image translation by use of deep neural networks: denoising, super-resolution, modality conversion, and reconstruction in medical imaging. Radiol Phys Technol 2019;12:235-48.

49. West JB. Respiratory physiology. The essentials. 1st ed. Philadelphia: Lippincott Williams & Wilkins, 1974.